Title: Climate explains geographic and temporal variation in mosquito-borne disease dynamics on two continents

Jamie M. Caldwell[1], A. Desiree LaBeaud[2], Eric F. Lambin[3,4], Anna M. Stewart-Ibarra[5,6], Bryson A. Ndenga[7], Francis M. Mutuku[8], Amy R. Krystosik[2], Efraín Beltrán Ayala[9], Assaf Anyamba[10], Mercy J. Borbor-Cordova[11], Richard Damoah[12], Elysse N. Grossi-Soyster[2], Froilán Heras Heras[13], Harun N. Ngugi[14,15], Sadie J. Ryan[16-18], Melisa M. Shah[19], Rachel Sippy[13,20,21], Erin A. Mordecai[1]

[1] Department of Biology, Stanford University, 371 Serra Mall, Stanford, California, USA

[2] Department of Pediatrics, Division of Infectious Diseases, Stanford University, 300 Pasteur Drive, Stanford, California, USA

[3] School of Earth, Energy & Environmental Sciences, and Woods Institute for the Environment, Stanford University, Stanford, California 94305, USA.

[4] Georges Lemaître Earth and Climate Research Centre, Earth and Life Institute, Université catholique de Louvain, 1348 Louvain-la-Neuve, Belgium.

[5] Department of Medicine and Department of Public Health and Preventative Medicine, SUNY Upstate Medical University, Syracuse, NY, USA

[6] InterAmerican Institute for Global Change Research (IAI), Montevideo, Uruguay

[7] Centre for Global Health Research, Kenya Medical Research Institute, Kisumu, Kenya

[8] Department of environment and health sciences, technical university of Mombasa, Mombasa, Kenya

[9] Technical University of Machala, Machala, Ecuador

[10] Universities Space Research Association and NASA Goddard Space Flight Center, Greenbelt, MD, USA.

[11] Facultad de Ingeniería Marítima y Ciencias del Mar, Escuela Superior Politécnica del Litoral, ESPOL, Guayaquil, Ecuador

[12] Morgan State University and NASA Goddard Space Flight Center, Greenbelt, MD, USA.

[13] Center for Research SUNY-Upstate-Teófilo Dávila Hospital, Machala, Ecuador

[14] Department of Biological Sciences, Chuka University, Chuka, Kenya

[15] Department of Zoology, School of Biological Sciences University of Nairobi, Nairobi, Kenya

[16] Emerging Pathogens Institute, University of Florida, Gainesville, Florida

[17] Quantitative Disease Ecology and Conservation (QDEC) Lab, Department of Geography, University of Florida, Gainesville, Florida;

[18] School of Life Sciences, University of KwaZulu, Natal, South Africa

[19] Department of Medicine, Division of Infectious Diseases, Stanford University, 300 Pasteur Drive, Stanford, California, USA

[20] Institute for Global Health and Translational Science, SUNY-Upstate Medical University, Syracuse, NY, USA

[21] Department of Medical Geography, University of Florida, Gainesville, FL, USA

Abstract:

Climate drives population dynamics, but when the underlying mechanisms are unresolved, studies can lead to seemingly context-dependent effects of climate on natural populations. For climate-sensitive vector-borne diseases such as dengue, chikungunya, and Zika, climate appears to have opposing effects in different contexts. In this study, our objective was to test the extent to which a mathematical model, parameterized with climate-driven mosquito physiology measured in laboratory studies, predicts observed vector and disease dynamics in the field across ecologically and culturally distinct settings in Ecuador and Kenya. The model incorporates different rainfall functions and time lags. We show that the climate-driven model captures three key epidemic characteristics across settings: the number, timing, and duration of outbreaks. In addition, the model generates a range of disease dynamics consistent with observations of *Aedes aegypti* abundances and laboratory-confirmed arboviral incidence with varying levels of accuracy (28 – 85% for vector dynamics, 36 – 88% for human disease dynamics). Further, we find that the model predicted vector dynamics better in sites with a smaller proportion of young children in the population, lower mean temperature, and a larger proportion of homes without window screens and made of cement. A mechanistic model with limited calibration to local data that robustly captures the influence of climate on viruses transmitted by *Aedes aegypti* provides critical information to help guide future intervention efforts and improve climate change predictions.

Introduction:

Climate is a major driver of species interactions and population dynamics, but the mechanisms underlying the ecological effects of climate are often poorly understood and rarely tested in the field [1]. One of the primary ways that climate impacts populations is through its effects on species' vital rates [2]. However, the effects of climate on population dynamics may appear context dependent in the field because multiple climate variables can act synergistically, with each climate variable potentially affecting multiple vital rates, and their impacts may be nonlinear, changing direction and relative importance across a gradient of conditions [3,4]. Therefore, paradoxically, while climate is thought to be one of the most pervasive drivers of ecological processes, its directional and dynamical effects on systems are often poorly understood and difficult to predict. Vector-borne diseases provide an interesting case study to test whether climate sensitive traits measured in controlled, laboratory settings can reproduce the wide range of dynamics observed in the field. For example, transmission of mosquito-borne viral (arboviral) diseases such as dengue, chikungunya, and Zika occur along a spectrum from low levels of year-round endemic transmission [5] to large seasonal or interannual outbreaks [6]. We hypothesize that important features of these differing dynamics arise due to regional or seasonal differences in climate, where the magnitude and direction of the effects of climate on vector and disease dynamics differ [7–12].

Understanding the mechanisms that drive disease dynamics can help address two critically important research priorities for arboviruses like dengue, chikungunya, and Zika: assessing intervention strategies and projecting climate change impacts on disease

dynamics. While phenomenological models often replicate arboviral disease dynamics remarkably well [13], mechanistic models that do not rely on local data for calibration and capture mosquito population dynamics and interactions between mosquitoes and humans will provide more realistic predictions for epidemic dynamics across a broad range of transmission settings. With no widely available vaccine, vector control (e.g., larvicides, *Wolbachia*-infected mosquito releases) remains the primary method for preventing arboviral disease transmission, and, like other vector-borne diseases with complex transmission dynamics, model simulations can help guide effective intervention efforts [14,15]. Further, mechanistic models are better suited to predict how climate change will impact future disease burden and distribution, as projected climate conditions are outside the current arboviral climate niche space [16]. Despite the potential usefulness of mechanistic approaches, validation with vector and disease data are limited, raising an important question about which epidemic characteristics, if any, we should expect a model to capture when the model was parameterized with data that is on different scales (e.g., individuals versus populations) and independent from the transmission system we wish to predict. Thus, because we cannot study epidemic dynamics in every possible transmission setting, it becomes important to understand the extent to which models derived from fundamental and laboratory-measured traits explain disease dynamics across diverse settings.

We hypothesize that a climate-driven mechanistic model with limited calibration should capture many important characteristics of disease dynamics for dengue, chikungunya, and Zika because of the ecology of *Aedes aegypti*, the primary disease vector. *Ae. aegypti* are

anthropophilic, globally distributed mosquitoes that breed in artificial containers with standing water [17,18]. All mosquito and parasite traits that are important for transmission and linked to metabolism, such as reproduction, development, survival, biting rate, and extrinsic incubation period, are temperature dependent with an intermediate thermal optimum [19–21]. Humidity is positively associated with mosquito survival because the high surface area to volume ratio of mosquitoes exposes them to desiccation [22,23]. Standing water from rainfall provides essential larval and pupal habitat for mosquitoes, but the relationship is complex because heavy rainfall can flush away breeding habitats [24–26] and water storage practices during drought can increase water availability, mosquito abundance, and contact between mosquitoes and people [27–29]. A previous simulation study predicted that in settings with suitable climate for transmission throughout the year (e.g., mean temperature = 25°C; range = 20 – 30°C), temperature drives the timing and duration of outbreaks, but not the maximum number of infections or final epidemic size [30]. This finding suggests that a model that incorporates temperature-dependent vector traits should capture some important epidemic characteristics.

In this study, our goal was to test the extent to which climate-driven mosquito traits drive disease dynamics across two geographically distinct regions and to characterize additional climatological, ecological, and social factors that may mediate the effects of climate on disease dynamics. We built on previous mechanistic and semi-mechanistic models that incorporate the *Aedes* mosquito life cycle and human disease dynamics [30–35] by combining a suite of temperature, humidity, and rainfall dependent trait functions

into one epidemiological model. We validated the model with *Ae. aegypti* abundances and laboratory-confirmed dengue, chikungunya, and Zika cases from two equatorial countries with distinct socioeconomic, geographic, cultural, and disease transmission settings: Ecuador and Kenya (Fig. 1, Table 1). The study sites within each country were distributed across a gradient of temperature, humidity, and rainfall. Previous studies have found that *Ae. aegypti* and dengue were positively associated with warm and wet conditions in Ecuador and Kenya [6,36–38], although other *Ae. aegpyti*-vectored arboviruses in Kenya such as chikungunya have been associated with warm and dry conditions [39]. Both countries have all four dengue serotypes circulating and have recently experienced outbreaks of chikungunya; yet, arboviral transmission dynamics differ in each country. In Ecuador, dengue is a re-emerging disease with large seasonal epidemics that frequently result in severe dengue [6]; by contrast, in Kenya, dengue is transmitted at low levels year-round [5] and intermittent self-limiting outbreaks often go undetected [40]. Further, compared with South America, severe dengue is rare in sub-Saharan Africa, perhaps because African strains of *Ae. aegpyti* have lower susceptibility to all four dengue serotypes [41], and/or because people of African ancestry are less susceptible to severe dengue [42].

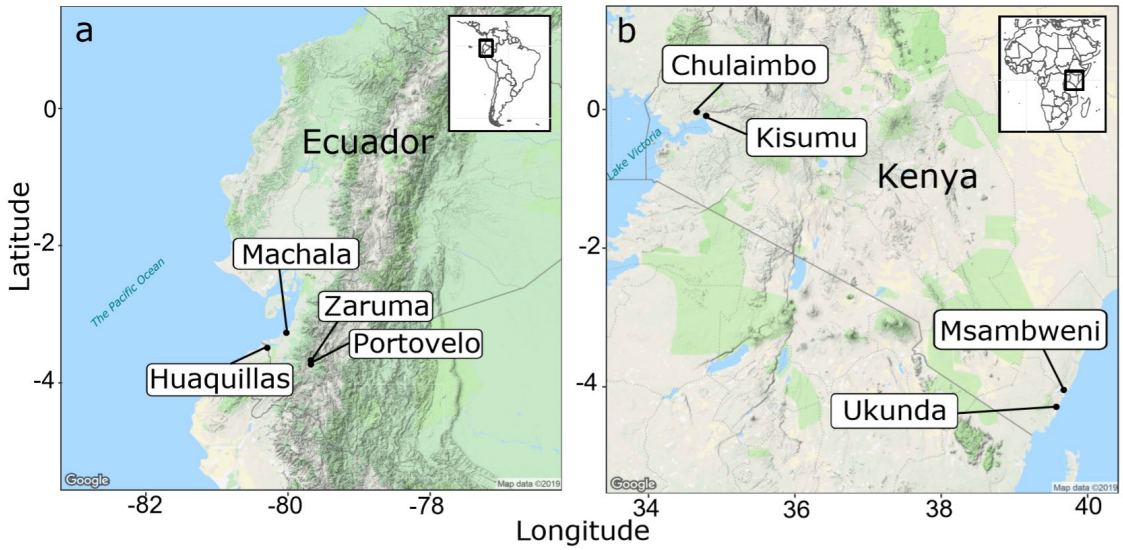

157

158 **Figure 1: Study sites within two equatorial countries:** (a) Ecuador in South America

159 and (b) Kenya in East Africa.

160

161 **Table 1: Study sites differ geographically, climatologically, and socioeconomically.**

162 [1]Mean annual normalized difference vegetation index (NDVI) is a proxy for

163 photosynthesis and measured as a difference in spectral reflectance in the visible and

164 near-infrared regions from NASA/NOAA MODIS (MOD13A1) [43]. [2]Dominant land

165 cover type is measured and classified from spectral and temporal features from

166 NASA/NOAA MODIS (MCD12Q1) [44]. Land cover types include (9) Tree cover 10 -

167 30%, (10) Dominated by herbaceous annuals, (13) >30% impervious surface area, and

168 (14) 40 - 60% mosaics of small-scale cultivation. Bed net use represents availability of

169 and/or willingness to adopt intervention strategies for preventing infection rather than a

170 direct adaptive response to preventing infection by day-biting *Ae. aegpyti* mosquitoes.

171

	Huaquillas, Ecuador	Machala, Ecuador	Portovelo, Ecuador	Zaruma, Ecuador	Chulaimbo, Kenya	Kisumu, Kenya	Msmabweni, Kenya	Ukunda, Kenya
Site characteristics								
Elevation (m)	15	6	645	1,155	1,328	1,100	4	8
Location	Coastal	Coastal	Inland	Inland	Inland	Inland	Coastal	Coastal
Mean annual NDVI[1]	0.22	0.12	0.61	0.57	0.63	0.35	0.33	0.52
Dominant land cover type[2]	13	13	9	10	14	13	13	10
Climate								
Mean temperature (°C)	26	26	25	22	24	26	28	28
Mean relative humidity (%)	81	84	81	86	69	50	76	78
Mean annual rainfall (mm)	317	669	500	1115	1125	810	1048	922
Demographics								
Human population size	57,366	279,887	13,673	25,615	7,304	491,893	15,371	80,193
Population <5 years (%)	10	9	9	8	12	12	13	14
Population of African ancestry (%)	5.1	6.0	3.3	2.9	100.0	100.0	100.0	100.0
Housing quality (% houses)								
Piped water inside home	90	91	100	96	2	4	3	11
No screens on windows	7	60	91	99	74	78	43	21
House materials (cement/mud/wood)	87/5/0	87/8/5	95/0/5	93/1/1	29/70/0	77/17/0	38/62/0	51/47/0
Exposure, vulnerability, and adaptive capacity								
Arboviruses present	dengue, chikungunya, Zika				>200 documented including dengue, chikungunya, Yellow fever, Rift Valley fever, West Nile fever, O'nyong-nyong			
Insecticide use (% houses)	19	28	46	37	0	0	11	55
Bednet use (% houses)	77	55	15	21	93	92	0	96
Other vector control strategies used	Ultra-low volume fumigation with malathion (organophosphate) and community mobilization to eliminate larval habitats				Mosquito coils			
Annual gross domestic product by country (2018)	$177 billion USD				$85.98 billion USD			

Results:

Capturing key epidemic characteristics

The dynamic susceptible, exposed, infectious – susceptible, exposed, infectious, removed (SEI-SEIR) compartmental model parameterized with temperature-, humidity-, and rainfall-dependent mosquito life history traits (Fig. 2) reproduced three key characteristics of epidemics: number of outbreaks, timing of outbreak peak, and duration

of outbreaks. We defined an outbreak as a continuous time period with peak cases exceeding the median number of cases (predicted or observed) plus one standard deviation within a site. Across all sites, the number of outbreaks predicted by the model closely matched the number of outbreaks observed ($R^2 = 0.79$, $p < 0.01$; Fig. 3a). Supporting our *a priori* expectations based on a previous simulation study [30], we found that the climate-driven model predicted peak timing of outbreaks ($R^2 = 0.71$, $p < 0.01$; Fig. 3b) and outbreak duration ($R^2 = 0.51$, $p < 0.01$; Fig. 3c) well but did not predict the final outbreak size (Fig. 3d) or maximum number of infections (Fig. 3e) across sites. Overall, it was more slightly common for the model to predict outbreaks that were not observed (N = 4) than to predict no outbreak when one occurred (N = 3). The model may miss an outbreak (i.e., false negatives) when, for example, suitable climate occurs but the pathogen is not introduced or the susceptible population is depleted from previous outbreaks.

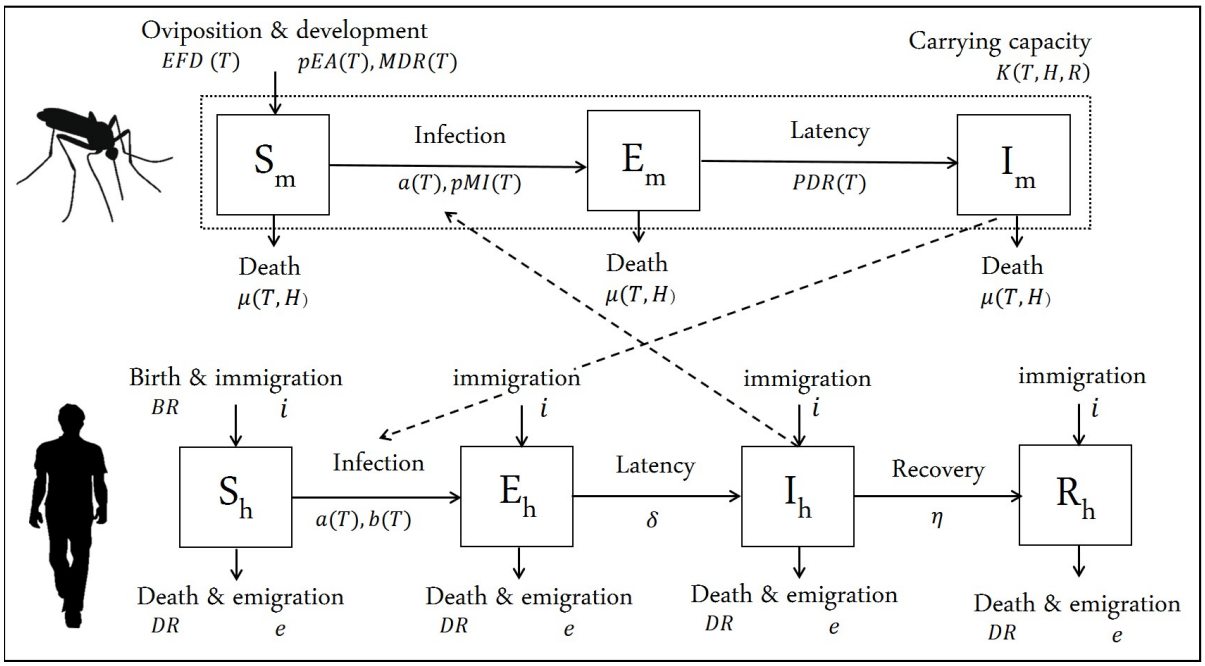

Figure 2: SEI-SEIR epidemiological model framework. The mosquito population is split among susceptible (S_m), exposed (E_m), and infectious (I_m) compartments (squares) and the human population is split among susceptible (S_h), exposed (E_h), infectious (I_h), and recovered (R_h) compartments. Solid arrows indicate the direction individuals can move between classes and dashed arrows indicate the direction of transmission. Transitions among compartments are labeled by the appropriate processes and corresponding rate parameters (see Methods for parameter definitions and more detail). Rate parameters with a T, H, and R are temperature-, humidity-, and rainfall-dependent, respectively. The total adult mosquito population (S_m, E_m, and I_m compartments; dotted rectangle) is maintained at an abundance less than or equal to the mosquito carrying capacity.

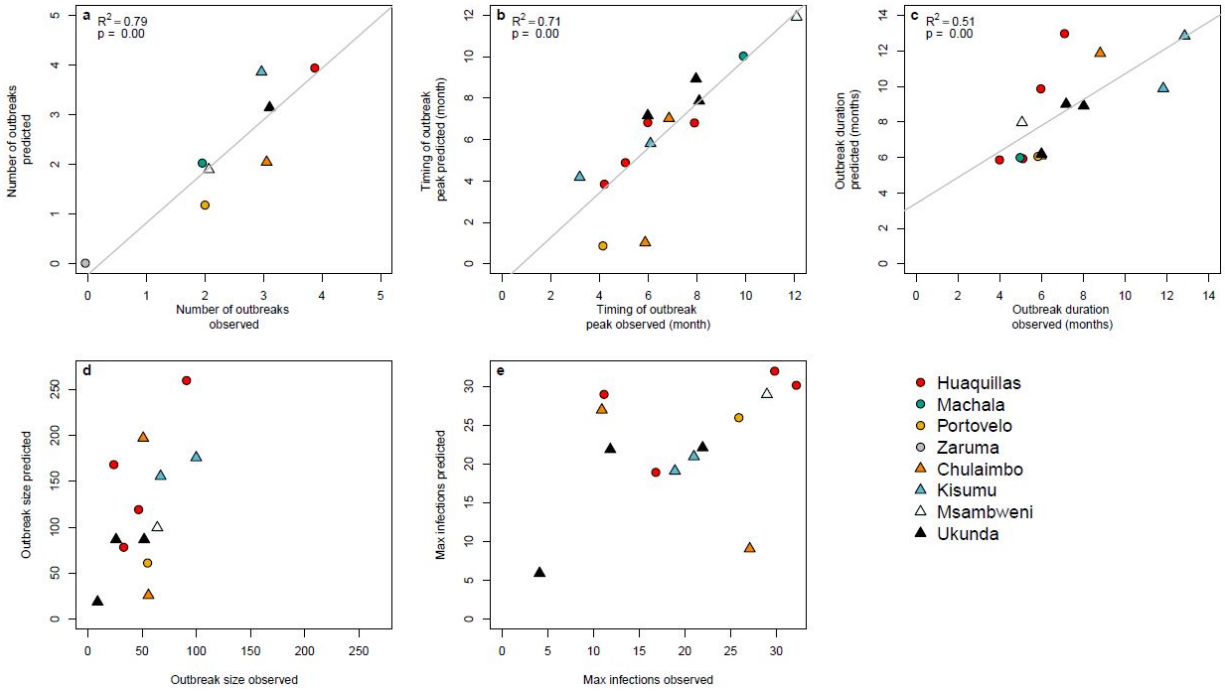

Figure 3: Model predictions for the number, timing, and duration of arboviral outbreaks closely matched field observations. Scatterplots show model predictions

versus observations for different epidemic characteristics. (a) Number of outbreaks indicates the total number of predicted and observed outbreaks in a site over the study period. (b) Timing of outbreak peak, (c) outbreak duration, (d) outbreak size, and (e) maximum infections (e.g., max I_h during an outbreak) correspond to individual outbreaks where model predictions and observations overlapped in time (including offset outbreaks if discernable), therefore, some plots show multiple data points per site. Outbreaks are colored by site with different symbols for Ecuador (circles) and Kenya (triangles). We show regression lines and associated statistics for statistically significant relationships. For visualization purposes, we jittered the data points to show overlapping data and we excluded data from Machala in plots (d) outbreak size and (e) maximum infections because the magnitude differed substantially from all other sites.

Capturing spatio-temporal disease dynamics across sites

The SEI-SEIR model generated mosquito and disease dynamics that better reflected observed dynamics in some sites than others (Fig. 4, Table 2). Model-predicted mosquito abundances were significantly correlated with field-collected observations of mosquito abundances in all eight study sites, explaining 28 – 85% of site-level variation through time based on pairwise correlations with an adjusted p-value for time series data (following [45]). Based on surveys conducted across all vector life stages in Kenya (only adult mosquitoes were collected in the Ecuador surveys), the SEI-SEIR model explained variation in the abundance of adult mosquitoes (28 – 63%) better than pupae (25 – 32%), late instars (30 – 33%), early instars (20 – 36%), and eggs (33 – 55%), likely because the model did not explicitly incorporate other mosquito life history stages. Model-predicted

disease cases were significantly correlated with laboratory-confirmed arboviral incidence in seven of the eight study sites, explaining 44 – 88% of site-level variation through time (within sites with statistically significant pairwise correlations). We confirmed that the predicted dynamics were stable with sensitivity analyses to initial conditions (see Methods), as emerging diseases can display chaotic dynamics due to a high sensitivity to initial conditions. Overall, the model reproduced disease dynamics slightly better for sites in Ecuador compared with Kenya.

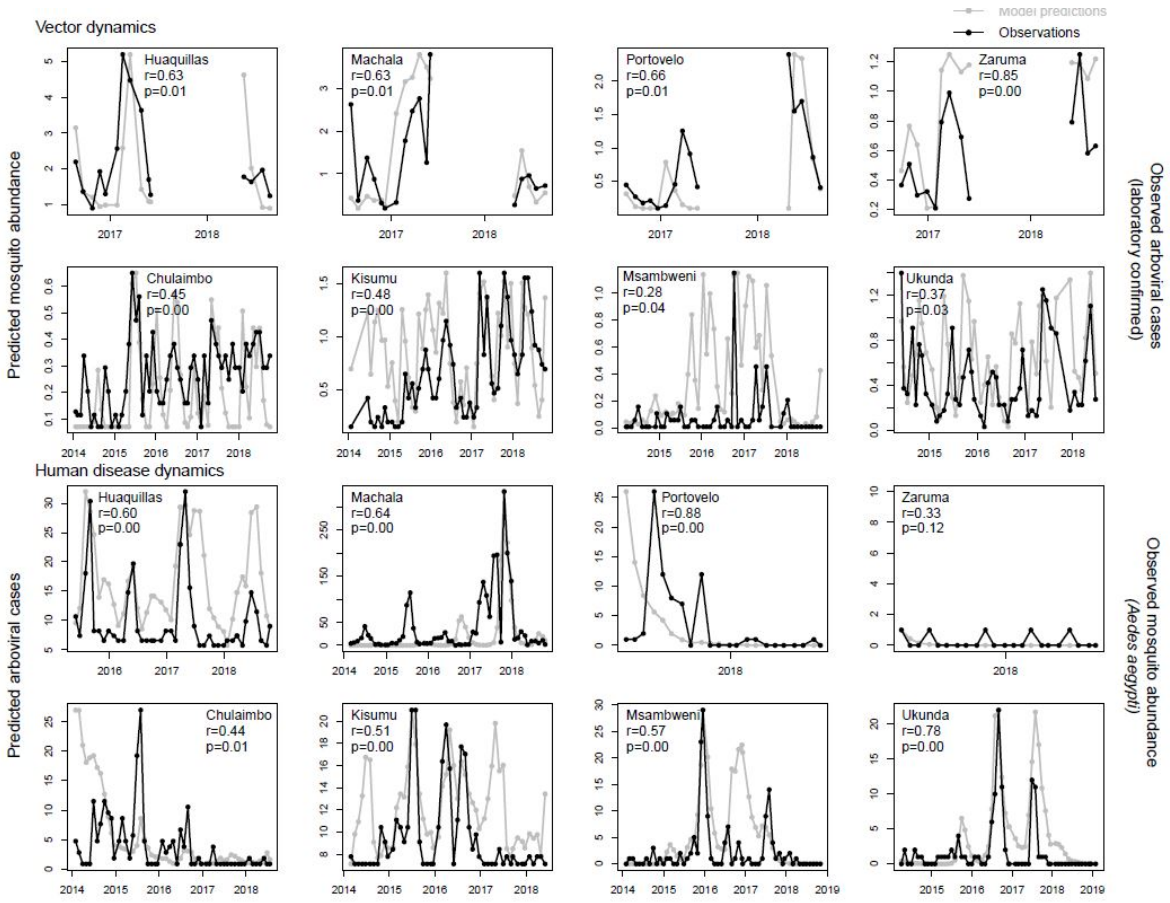

Figure 4: Model predicts vector and human disease dynamics better in some settings than others. Each plot shows the time series of SEI-SEIR model predictions (grey dots connected by grey lines) and field observations (black dots connected by black lines) for

vector (top two rows) and human disease (bottom two rows) dynamics for each study site with the pairwise correlation (r) and adjusted p-value (p). We calculated observed mosquito abundances as the mean number of adult *Ae. aegypti* per house, month, year, and site. We calculated observed arboviral cases as the total number of laboratory-confirmed dengue (any serotype), chikungunya, and Zika cases per month, year, and site; six of the eight study sites only included dengue cases (see Methods). The first and third rows show sites in Ecuador and the second and fourth rows show sites in Kenya. We show uncertainty in model predictions in Figs. S1-2.

Table 2: Model predictions reflect a range of observed transmission dynamics when incorporating different rainfall functions and time lags across sites. For each study site, we calculated pairwise correlations between time series of field observations (*Ae. aegypti* abundances or arboviral cases) and time series of model predictions for the SEI-SEIR model with one of three rain functions for mosquito carrying capacity (Brière, Inverse, or Quadratic) and six time lags (0-5 months). This table shows specifications for the model (e.g., rain function and time lag) with the highest pairwise correlation value, r, for each study site and observation type (vectors or human disease cases), as well as the statistical significance of the correlation value (adjusted p-value) based on the Modified Chelton method [45] to account for temporal autocorrelation.

	Vector dynamics				Human disease dynamics			
Site	Rainfall function	r	Adjusted p-value	Lag (months)	Rainfall function	r	Adjusted p-value	Lag (months)
Huaquillas, Ecuador	Quadratic	0.63	0.01	1	Inverse	0.60	0.00	2
Machala, Ecuador	Quadratic	0.63	0.01	0	Brière	0.64	0.00	4

Portovelo, Ecuador	Brière	0.66	0.01	1	Brière	0.88	0.00	3
Zaruma, Ecuador	Inverse	0.85	0.00	1	Inverse	0.33	0.12	0
Chulaimbo, Kenya	Inverse	0.45	0.00	1	Quadratic	0.36	0.02	4
Kisumu, Kenya	Brière	0.48	0.00	0	Quadratic	0.51	0.00	4
Msambweni, Kenya	Inverse	0.28	0.04	0	Inverse	0.57	0.00	3
Ukunda, Kenya	Inverse	0.37	0.03	1	Inverse	0.78	0.00	5

We found evidence that rainfall affects transmission through multiple mechanisms and at different time lags (Table 2). Since the effect of rainfall on mosquito abundances is not well understood, we simulated disease dynamics for each site three times, using one of three hypothesized rainfall relationships (Brière, inverse, and quadratic; Fig. S3). We determined the best rainfall function and time lag for each site based on the highest pairwise correlation value between model predictions and observations. The model with the exponentially decreasing inverse rain function (Fig. S3c), which indicates that mosquito abundances peak when there is no or low rainfall (likely as a result of water storage practices and/or unreliable water sources) described observed mosquito and disease dynamics most often, especially in the Kenya sites (Table 2), where household access to piped water is very low (Table 1). The left-skewed unimodal Brière rainfall function (Fig. S3a), which indicates that mosquito abundances increase with increasing rainfall until some threshold where flushing occurs, described disease dynamics in some settings, particularly in the Ecuador sites. The symmetric unimodal quadratic rainfall function (Fig. S3b), which indicates that mosquito abundances peak with intermediate amounts of rainfall and are reduced with low and high rainfall values, also described

disease dynamics in some settings. Interestingly, we did not find a single rainfall function that consistently described dynamics for mosquitoes or arboviral cases across study sites, or for both mosquitoes and arboviral cases within individual study sites (Table 2). In contrast, we did find some consistency with time lags. The model best predicted mosquito abundances in the same month or one month in the future. In more than half of the sites, the model best predicted human disease cases three to four months in the future, and in almost all sites at least two months in the future (the exception is Zaruma, where very few arbovirus cases were reported during the study period and were likely due to importation rather than local transmission). Given that multiple rainfall functions and time lags are supported by field data (even within the same study site), we propose a conceptual model that incorporates multiple pathways for rainfall to affect disease dynamics along a continuum of rainfall (Fig. 5), in contrast to distinct functional relationships for a given setting, which motivated the approach used in this study.

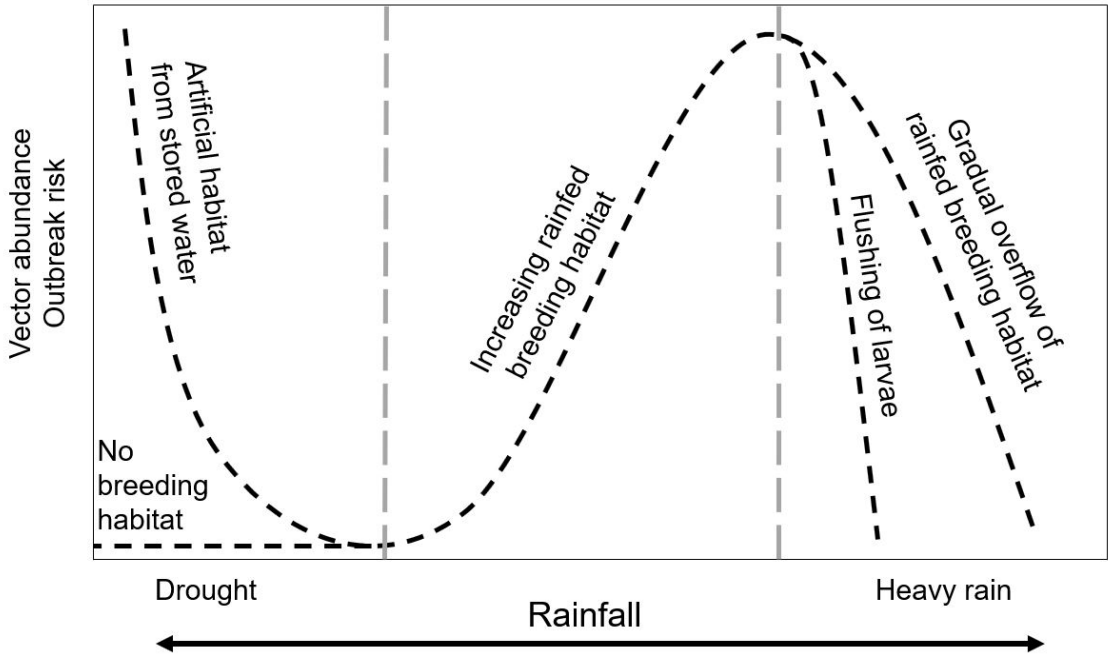

294

295 **Figure 5: Conceptual model for nonlinear functional relationships between rainfall**
296 **and vector abundance and arboviral outbreak risk.** Dashed lines show multiple
297 potential pathways for rainfall to affect transmission dynamics and include the functional
298 relationships supported in this study. Labels indicate the hypothesized mechanisms along
299 a gradient of rainfall. Adapted from [46].

300

301 ***Factors that mediate disease dynamics predictability***

302 The ability of the model to generate similar dynamics to those found in the field varied
303 with demography, housing quality, and climate. Although the sample size is small (N = 8
304 sites), we found that the SEI-SEIR model generally predicted vector dynamics better in
305 sites with a smaller proportion of young children in the population ($R^2 = 0.89$, $p < 0.01$;
306 Fig. 6a), lower mean temperature ($R^2 = 0.63$, $p < 0.05$; Fig. 6c), and a larger proportion of
307 homes with piped water ($R^2 = 0.76$, $p < 0.01$; Fig. 6b) and made of cement ($R^2 = 0.69$, p

< 0.05; Fig. 6d; list of all factors we assessed are provided in Table 1). Based on the range of mean temperatures at our study sites (22 – 28°C), our findings indicate that vector dynamics become less predictable as temperatures near the optimal temperature for transmission (derived in previous studies as 29°C) following the shape and slope in the R_0 curve (Fig. 7). This complements phenomenological models that have found minimal effects of temperature near the empirically derived thermal optima (Fig. 7). None of the socio-economic factors that we examined in this study (Table 1) explained variability in the pairwise correlations for human disease cases among sites.

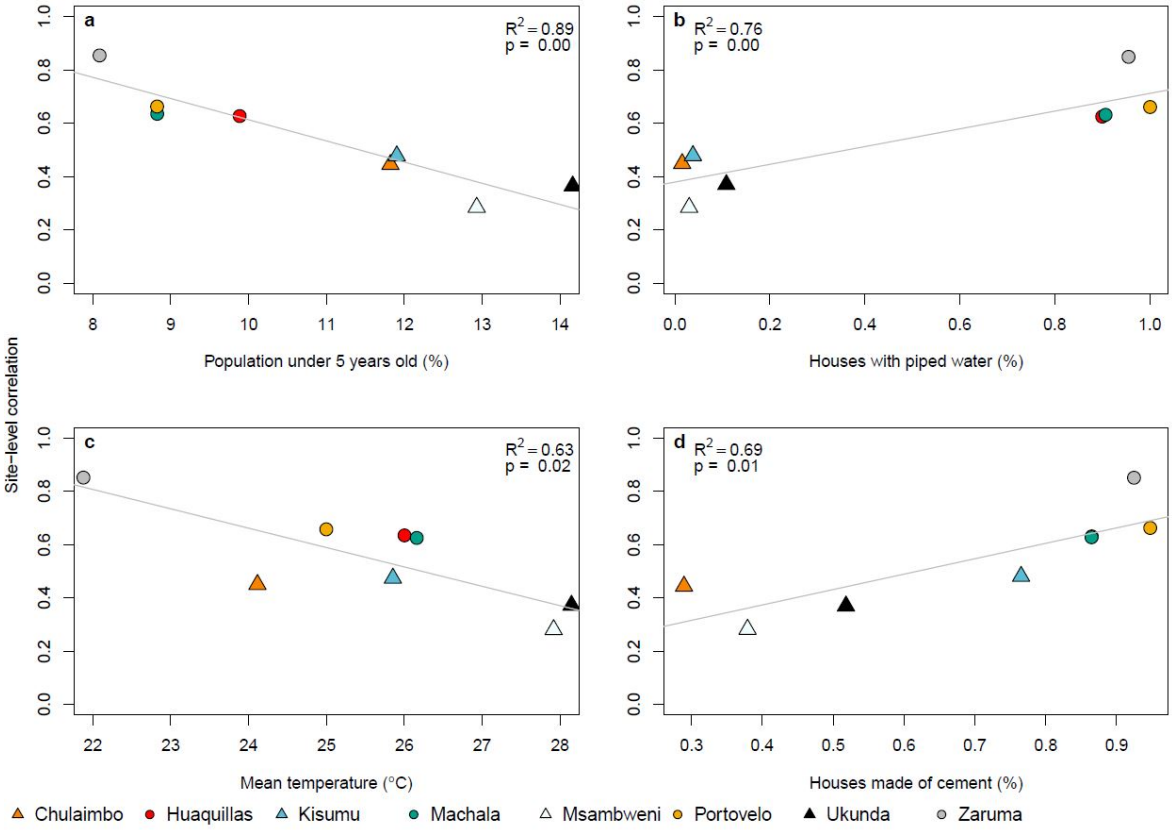

Figure 6: Demography, housing construction, and climate affect model predictive capacity for vectors. Factors that influence the predictability of vector dynamics include (a) proportion of the population under five years of age, (b) proportion of houses without screens, (c) mean temperature, and (d) proportion of houses made with cement (walls

and/or floors). Points indicate the pairwise correlation value for a single site (colors) with different symbols for Ecuador (circles) and Kenya (triangles). Each plot also shows the linear regression lines and associated statistics.

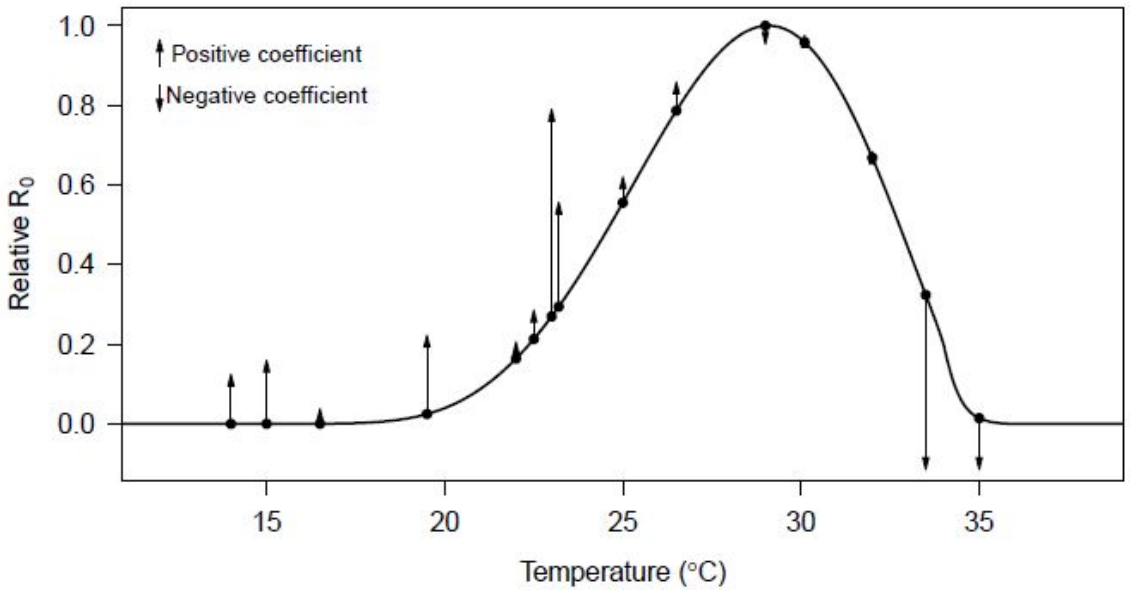

Figure 7: Independently predicted relative R_0 from a model derived from laboratory studies explains differences in the magnitude and direction of the effects of temperature on dengue transmission in the field across varied settings from previous studies. The black line shows the relative basic reproductive number (R_0, normalized to a 0-1 scale) plotted against temperature based on all temperature-dependent traits from [19] used in the SEI-SEIR model presented here. Points indicate mean temperature values from previous field-based statistical analyses that related dengue cases with minimum, maximum, or mean ambient temperature; arrows correspond to the direction (up = positive, down = negative) and relative effect size of the temperature – dengue relationship based on coefficient values from the following studies: [47,48,57,58,49–56]. See Methods and Table S1 for more detail. As expected, the largest

observed positive effects of temperature occurred in the rapidly increasing portion of the R_0 curve (~22-25°C; consistent with findings in this study) and the largest observed negative effects occurred well above the predicted optimum, near the upper thermal limit (~33-35°C).

Discussion:

Directly observing the influence of climate on species interactions and population dynamics is often challenging because of interacting and nonlinear relationships. Here, we directly and quantitatively connect laboratory-based climate relationships to observed mosquito and disease dynamics in the field, supporting the mechanistic role of climate in these disease systems. The trait-based modeling approach captured several key epidemic characteristics and generated a range of disease dynamics along a spectrum of settings with low levels of transmission to seasonal outbreaks, helping to reconcile seemingly context dependent effects (i.e., opposite conclusions about the magnitude and direction of effects; Fig. 7) of climate on arboviral transmission dynamics from the literature [7–12,47].

The results of this study shed some light on the influence of climate in driving endemic versus epidemic dengue transmission. Although Ecuador typically experiences seasonal epidemics [6] and Kenya typically experiences low levels of year-round transmission [5], the sites within this study suggest that epidemic transmission is more common in settings with clear seasonality (e.g., coastal sites) whereas endemic transmission is more common in settings with more climate variability (e.g., inland sites), regardless of country. Coastal

sites experienced more regular seasonal climate cycles, likely because oceans buffer climate variability, and this seasonality corresponded with seasonal epidemics. In contrast, the inland sites experienced more day-to-day climate variability, which resulted in more fluctuations in disease cases. As a result, the occurrence and persistence of suitable temperature, rainfall, and humidity conditions enabling outbreaks were less regular in sites with more climate variability. The ability of the model to detect key epidemic characteristics across endemic and epidemic settings indicates that climate plays a major role in driving when outbreaks occur and how long they last.

Using field data on mosquitoes and disease cases from diverse settings and a model parameterized with data from other studies, we identified several key epidemic characteristics that we should (and should not) expect to capture in new settings. While we would never expect a perfect correlation between model predictions and observations, even if the model perfectly captured climate-host-vector dynamics because of the many additional factors that affect transmission in nature, our results indicate that a model with limited calibration can determine the number of outbreaks across settings remarkably well (Fig. 3a). This finding could be particularly useful for prioritizing surveillance or intervention activities across a range of a potential sites that would otherwise appear equal in their propensity for outbreaks (e.g., similar climate conditions). We also show that the model captures the peak timing of outbreaks (Fig. 3b) and outbreak duration (Fig. 3c) but not the final outbreak size (Fig. 3d) or maximum number of infections (Fig. 3e), supporting the hypothesis that the magnitude of disease cases during an outbreak in settings with year-round climate suitability for disease transmission are invariant to

383 temperature, as proposed by [30], likely because the magnitude of disease cases is
384 probably more strongly driven by the availability of susceptible hosts.
385
386 Given that the model generally did not predict the magnitude of outbreaks, we asked how
387 well the model reproduced vector and human disease dynamics (i.e., variation over time)
388 across sites and whether this relationship varied systematically with different socio-
389 economic factors. The range across sites of temporal correlations between model
390 predictions and observations (N = 8; Fig. 4, Table 2) provides an informative metric for
391 the proportion of true disease dynamics that we might expect to capture in new settings,
392 ranging from 28 – 88%. The correlations varied with demography, housing construction,
393 and climate (Fig. 6). The model may have better explained vector dynamics in locations
394 with a lower proportion of children under five years old for a variety of reasons,
395 including because bottom-heavy demographic pyramids are often associated with lower
396 socioeconomic status and higher mobility throughout the day. In addition to the
397 demographic makeup of sites, housing construction within sites also seems to modify
398 transmission dynamics: vector dynamics were less predictable in sites with more houses
399 with piped water and made of cement (Fig. 6b,d). These results suggest that piped water
400 may prevent additional contact between humans and mosquitoes associated with stored
401 water around the home. In addition, housing materials like cement that lower indoor
402 temperature could artificially decrease climate suitability for mosquitoes, thereby
403 decreasing the probability that mosquitoes will enter and bite people inside their homes.
404 Despite incorporating all known temperature-dependent mosquito traits into the SEI-
405 SEIR model, we still found vector dynamics became less predictable near the empirically

406 derived thermal optima for arboviral transmission (Figs. 6c, 7). This finding may be
407 associated with physiological or behavioral responses of mosquitoes to temperatures near
408 their thermal safety margin [59,60] and/or humans modifying their environment (as
409 described above) in locations optimal for transmission.
410
411 Across the study sites, we found support for three hypothesized relationships between
412 rainfall and mosquito carrying capacity as well as several time lags between model
413 predictions and disease observations. Support for multiple rainfall functions could
414 indicate that the effects of rainfall on immature habitat is highly heterogenous, which has
415 been found in previous research in Ecuador [27] and Kenya [61]. Alternatively, the
416 combination of multiple rainfall relationships and time lags could arise from nonlinear
417 and delayed effects of extreme climate such as droughts and floods. More specifically,
418 we hypothesize that there may be multiple mechanistic relationships for the effects of
419 rainfall on mosquito abundance and arboviral disease dynamics (Fig. 5), and they may act
420 on different time scales. For example, previous research indicated that dengue outbreaks
421 were more likely to occur four to five months after a drought and one month after
422 excessive rainfall and a statistical model that incorporated these duel exposure-lag-
423 response functions was highly effective at predicting dengue outbreaks in Barbados [62].
424 Further, if multiple rainfall relationships act in concert across varying time lags, this
425 would help to explain why many different time lags have been observed between rainfall
426 and arboviral dynamics in previous studies [6,27,51,63–65].
427

Future research can build on this study to improve our understanding of arboviral dynamics across settings. There were several factors that we did not include in this study, such as existing vector control programs, infrastructure, and preexisting immunity in the population. For instance, in Ecuador, factors such as distance to abandoned properties, interruptions in access to piped water, shaded patios, and use of vector control are documented to influence arbovirus transmission [66], whereas in the study sites in Kenya, factors associated with arboviral transmission are less well studied and there are currently no widely used vector control or local arboviral surveillance programs employed. Future studies could further improve the model by incorporating human immune dynamics associated with interactions among different dengue serotypes [67] or cross-reactivity among viral antibodies [68], differential susceptibility across human age classes [69], and heterogeneity in contact rates between mosquitoes and people based on human behavior and movement [70,71]. Further, as experimental data becomes available for trait estimates specific to chikungunya and Zika, this model could be partitioned to model each arboviral disease individually. This is likely to be an important addition as the different arboviruses tend to peak in different years, possibility due to differences in viral development rates and extrinsic incubation periods among arboviruses. Therefore, validating the model with all three arboviruses combined may oversimplify the complex interannual dynamics that arise due to competition among arboviruses in mosquitoes and humans. There were not enough data for chikungunya and Zika cases in this study to formally test such patterns. This study provides strong evidence that a trait-based model, parameterized independently from field data, can reproduce key epidemic characteristics and a range of spatiotemporal arboviral disease dynamics. Such mechanistic, climate-

451 driven models will become increasingly important to support public health efforts in the
452 face of novel climate regimes emerging due to climate change.
453
454 **Materials and Methods:**
455 Climate data
456 We collected *in situ* measurements of daily mean temperature, relative humidity, and
457 rainfall at each study site and interpolated missing data where necessary. We used
458 temperature and humidity measurements from HOBO loggers and rainfall measurements
459 from rain gauges for sites in Kenya. We used temperature, humidity, and rainfall
460 measurements from automatic weather stations operated by the National Institute of
461 Meteorology and Hydrology in Ecuador. For Kenya, we interpolated missing temperature
462 data from NOAA Global Surface Summary of the Day (Table S2, Fig. S4) and
463 interpolated missing rainfall data from NOAA Climate Prediction Center Africa Rainfall
464 Climatology dataset (Table S2, Fig. S5). For Ecuador, we interpolated missing
465 temperature (Table S2, Fig. S4) and rainfall (Table S2, Fig. S5) data using the nearest
466 study site where possible and otherwise based on long term mean values for the
467 corresponding Julian day. To interpolate missing data, we linearly regressed all
468 measurements taken on the same day in two datasets and then used the linear model to
469 interpolate temperature for the site with missing data based on the climate measurement
470 from the secondary source for the date when the data was missing (Figs. S4-5). For
471 rainfall, we first calculated a moving window of 14-day accumulated rainfall (which is
472 short enough to capture variability and seasonality in rainfall patterns and follows [72])
473 for each day before interpolation because modeled daily rainfall values are less reliable

than accumulated rainfall over a two week period. We interpolated 14-day cumulative rainfall for any day with a missing rainfall value in the prior 14 days. For both Kenya and Ecuador, we interpolated missing relative humidity data based on long term mean values for the corresponding Julian day (Table S2). We then calculated the saturation vapor pressure deficit (SVPD) from temperature and humidity to use in the humidity function because previous research suggests SVPD is a more informative measure of the effect of humidity on mosquito survival compared with relative humidity [73]. To calculate SVPD, we first calculated the saturation vapor pressure as:

$$SVP = 610.7 * 10^{7.5*T/(273.3+T)} \quad (1)$$

where (T) is temperature in degrees Celsius. We then calculated SVPD (in kilopascals) as

$$SVPD = 1 - \frac{RH}{100} * SVP \quad (2)$$

where RH is relative humidity. The final dataset had no missing values for temperature (Fig. S6), rainfall (Fig. S7), and humidity (Fig. S8).

Vector surveys

We collected, counted, sexed, and classified mosquitoes by species, and aggregated the data to mean number of *Aedes aegypti* per house, month, year, and site to account for differences in survey effort across months and sites. We collected adult mosquitoes using Prokopack aspirators [74]. In Ecuador, we collected mosquitoes from approximately 27 houses per site (range = 3-57 houses across four sites) every one-to-two weeks during three, four-month sampling periods between July 2016 and August 2018 (≈ 37 sampling weeks per site) to capture different parts of the transmission season. We aggregated the Ecuador vector data to monthly values (≈ 15 sampling months per site) to correspond

with the temporal resolution of surveys in Kenya. In Kenya, we collected mosquitoes from approximately 20 houses per site (range = 1-47 houses across four sites) every month between January 2014 and October 2018 (≈ 54 sampling months per site). In Kenya, we also collected pupae, late instars, and early instars from containers with standing water around the home and collected eggs by setting ovitraps for an average of four days in and around each house monthly. We brought pupae, late and early instars, and eggs to the insectary and reared them to adulthood to classify individuals by sex and species. All mosquito traps capture a small portion of the true mosquito population; therefore, using consistent trapping methods at the same locations through time allows us to compare relative mosquito population dynamics across study sites rather than the absolute magnitude of mosquito abundances.

Arboviral surveys

For Ecuador, we analyzed laboratory-confirmed dengue, chikungunya, and Zika cases provided by the Ministry of Health (MoH) of Ecuador. The MoH collects serum samples from a subset of people with suspected arbovirus infections, and samples are tested at the National Public Health Research Institute by molecular diagnostics (RT-PCR) or antibody tests (IgM ELISA for dengue), depending on the number of days of illness. Results are sent to the MoH Epidemiological Surveillance and Control National Directorate (SIVE Alerta system). Laboratory-confirmed dengue cases were available for all four sites from 2014 to 2018. Laboratory-confirmed chikungunya cases were available for Machala and Huaquillas from 2015 to 2018. Laboratory-confirmed Zika cases were available for Machala from 2016 to 2018.

For Kenya, we used laboratory-confirmed dengue cases aggregated by site and month between 2014 and 2018 collected in a passive surveillance study on childhood febrile illness in Kenya (NIH R01AI102918, PI: ADL). The study population consisted of 7,653 children less than 18 years of age with undifferentiated febrile illness. Children with fever enrolled in the study when attending outpatient care in one of the four study sites (Mbaka Oromo Health Centre in Chulaimbo, Obama Children's Hospital in Kisumu, Msambweni District Hospital in Msambweni, and Ukunda/Diani Health Center in Ukunda). Local health officers collected comprehensive clinical and demographic data and phlebotomy at the initial visit. We tested each child's blood for dengue viremia by molecular diagnostics (conventional PCR [75] or targeted multiplexed real-time PCR when available [76]), or serologic conversion between an initial and a follow up visit (IgG ELISA [77]).

SEI-SEIR model

We adapted an SEI-SEIR model parameterized for dengue transmission in *Ae. aegypti* mosquitoes [30] to simulate mosquito abundance and arboviral cases through time based on daily weather conditions in eight study locations. The model (equations 3-9; Fig. 2), created independently from the observed data described above, allows mosquito life history traits and viral development rate to vary with temperature (T) following [30], mosquito carrying capacity to vary with accumulated 14-day rainfall (R) following [72], and mosquito mortality to vary with humidity (i.e., saturation vapor pressure deficit) (H) following [73].

$$\frac{dS_m}{dt} = \varphi(T,H) * \frac{1}{\mu(T,H)} * N_m * \left(1 - \frac{N_m}{K(T,R,H)}\right) - \left(a(T) * pMI(T) * \frac{I_h}{N_h} + \mu(T,H)\right) * S_m \quad (3)$$

$$\frac{dE_m}{dt} = a(T) * pMI(T) * \frac{I_h}{N_h} * S_m - \left(PDR(T) + \mu(T,H)\right) * E_m \quad (4)$$

$$\frac{dI_m}{dt} = PDR(T) * E_m - \mu(T,H) * I_m \quad (5)$$

$$\frac{dS_h}{dt} = -a(T) * b(T) * \frac{I_m}{N_h} * S_h + BR * S_h - DR * S_h + ie * N_h - ie * S_h \quad (6)$$

$$\frac{dE_h}{dt} = a(T) * b(T) * \frac{I_m}{N_h} * S_h - \delta * E_h - DR * E_h - ie * E_h \quad (7)$$

$$\frac{dI_h}{dt} = \delta * E_h - \eta * I_h - DR * I_h - ie * I_h \quad (8)$$

$$\frac{dR_h}{dt} = \eta * I_h - DR * R_h - ie * R_h \quad (9)$$

where

$$\varphi(T,H) = EFD(T) * pEA(T) * MDR(T) \quad (10)$$

The adult mosquito population (N_m) is separated into susceptible (S_m), exposed (E_m), and infectious (I_m) compartments and the human population (N_h) is separated into susceptible (S_h), exposed (E_h), infectious (I_h), and recovered (R_h) compartments (Fig. 2). Climate-independent model parameters (Table 3) include the intrinsic incubation period (δ), human infectivity period (η), birth rate (BR), death rate (DR), and immigration/emigration rate (ie). The temperature-dependent SEI-SEIR model was developed by Huber et al. [30] and allows mosquito life history traits and viral development rate to vary according to thermal response curves fit from data derived in laboratory experiments conducted at constant temperatures (Table 3). Although laboratory experiments do not reflect real-world conditions, the physiological responses measured are biologically meaningful. The temperature-dependent traits include eggs laid per female per day (EFD), the probability of egg-to-adult survival (pEA), mosquito development rate (MDR), mosquito mortality rate (lifespan^{-1}; μ), biting rate (a), probability of mosquito infection per bite on an infectious

host (pMI), parasite development rate (PDR), and probability of mosquito infectiousness given an infectious bite (b). We modified the mosquito mortality rate equation to vary as a function of temperature and humidity by fitting a spline model based on a pooled survival analysis of *Ae. aegypti* [73] (Fig. S9):

$$\mu(T,H) = \frac{1}{c * (T - T_0) * (T - T_m)} + (1 - (0.01 + 2.01 * H)) * y \qquad H < 1 \qquad (11)$$

$$\mu(T,H) = \frac{1}{c * (T - T_0) * (T - T_m)} + (1 - (1.22 + 0.27 * H)) * y \qquad H \geq 1 \qquad (12)$$

where the rate constant (c), minimum temperature (T_0), and maximum temperature (T_m) equal -1.24, 16.63, and 31.85 respectively (Table 4), humidity (H) is the saturation vapor pressure deficit, and y is a scaling factor that we set to 0.005 and 0.01, respectively, to restrict mosquito mortality rates within the range of mortality rates estimated by other studies [19,73]. The linear humidity function has a steeper slope at lower humidity values (equation 11) compared with higher humidity values (equation 12) based on previous research [73] (Fig. S9).

We modeled adult mosquito carrying capacity, K, as a modified Arrhenius equation following [30,78]:

$$K(T,H,R) = \frac{EFD(T_0) * pEA(T_0) * MDR(T_0) * \mu(T_0,H_0)^{-1} - \mu(T_0,H_0)}{EFD(T_0) * pEA(T_0) * MDR(T_0) * \mu(T_0,H_0)^{-1}} * N_{m.max} \qquad (13)$$

$$* e^{\frac{-E_A * (T - T_0)^2}{K_B * (T + 273) * (T_0 + 273)}} * f(R)$$

with T_0 and H_0 set to the temperature and humidity where carrying capacity is greatest (i.e., physiological optimal conditions from laboratory experiments; 29°C and 6 kPA), $N_{m.max}$ set to the maximum possible mosquito abundance in a population (twice the human population size following [30]), and the Boltzmann constant, (K_B), is 8.617 x 10^{-5} eV/K.

We set the activation energy, E_A, as 0.05 based on [30]. Since there were no experimental data from which to derive the functional response of mosquito carrying capacity across a gradient of rainfall values, we tested several functional relationships based on hypothesized biological relationships between freshwater availability and immature mosquito breeding habitat, modeling the effect of rainfall on carrying capacity, $f(R)$, as either:

$$f(R_{\text{Brière}}) = c * R * (R - R_{min}) * \sqrt{(R_{max} - R)} * z \quad (14)$$

$$f(R_{Quadratic}) = c * (R - R_{min}) * (R - R_{max}) * z \quad (15)$$

$$f(R_{\text{Inverse}}) = \frac{1}{R} * z \quad (16)$$

where minimum rainfall (R_{min}) equaled 1 mm and maximum rainfall (R_{max}) equaled 123 mm based on the high probability of flushing [26]. The quadratic function is similar to the rainfall function found in [26] and the inverse function is based on the rainfall function used in [72]. We used rate constants (c) of $7.86e^{-5}$ and $-5.99e^{-3}$ for the Brière and quadratic functions respectively, based on rate constants for other parameters with similar functional forms (Table 4). We also included a scaling factor, z (0. 28, 0.025, and 0.60 respectively), to restrict the maximum carrying capacity to produce model outputs based on a subsample of the total population for comparison with observations. Since the rate constant, c, is multiplied by z, inferring the exact value of c is not necessary because it is scaled by z. The scaling factor could be removed from the model to simulate dynamics in the total population.

Table 3: Values of temperature-invariant parameters used in the model. We derived daily birth and death rates in the model by dividing the per capita birth and death rates by 360 days. The World Bank Open Data can be found at https://data.worldbank.org/.

Parameter	Definition	Value	Source
δ^{-1}	Intrinsic incubation period (days)	5.9	[30]
η^{-1}	Human infectivity period (days)	5.0	[30]
BR	Annual birth rate (per 1000 people)	31.782 (Ecuador) 20.175 (Kenya)	The World Bank Open Data
DR	Annual death rate (per 1000 people)	5.284 (Ecuador) 5.121 (Kenya)	The World Bank Open Data
ie	Immigration/emigration rate	0.01	Expert opinion

Table 4: Fitted thermal responses for *Ae. aegypti* life history traits. Traits were fit to a Brière $[cT(T-T_0)(T_m-T)^{\frac{1}{2}}]$ or a quadratic $[c(T-T_m)(T-T_0)]$ function where T represents temperature. T_0 and T_m are the critical thermal minimum and maximum, respectively, and c is the rate constant. Thermal responses were fit by [19] and also used in [30]. Parasite development rate was measured as the virus extrinsic incubation rate.

Trait	Definition	Function	c	T_0	T_m
a	Biting rate (day^{-1})	Brière	2.71×10^{-04}	14.67	41.00
EFD	Eggs laid per female per day	Brière	2.08×10^{-02}	14.06	32.03
pEA	Probability of mosquito egg-to-adult survival	Quadratic	-3.36×10^{-03}	7.68	38.31
MDR	Mosquito egg-to-adult development rate (day^{-1})	Brière	1.49×10^{-04}	15.12	37.67
Lf	Adult mosquito lifespan (days)	Quadratic	-1.24	16.63	31.85
b	Probability of mosquito infectiousness	Brière	9.86×10^{-04}	12.05	32.79
pMI	Probability of mosquito infection	Brière	5.23×10^{-04}	1.51	34.74
PDR	Parasite development rate (day^{-1})	Brière	1.04×10^{-04}	11.50	38.97

To initiate the model, we used site-specific values for human population size and randomly selected one set of values for all sites for the proportion of mosquitoes and humans in each compartment. For Ecuador, we used population estimates from official population projections produced by Proyección de la Población Ecuatoriana, por años calendario, según cantones 2010-2020 (https://www.ecuadorencifras.gob.ec/proyecciones-poblacionales/) with population sizes of 57,366, 279,887, 13,673, and 25,615 for Huaquillas, Machala, Portovelo, and Zaruma, respectively, based on 2017 projections. For Kenya, we estimated the population sizes

622 served by each outpatient care facility by creating a polygon around all the geolocations
623 of study participants' homes enrolled at each outpatient care facility and summed
624 population count data from NASA's Socioeconomic Data and Applications Center
625 Gridded Population of the World v4 (https://doi.org/10.7927/H4JW8BX5) within each
626 polygon using ArcGIS v 10.4.1. We estimated population sizes of 7,304, 547,557,
627 240,698, and 154,048 for Chulaimbo, Kisumu, Msambweni, and Ukunda, respectively.
628 We set the ratio of mosquitoes to humans to two, following [30]. We used the following
629 values as the initial proportion of mosquitoes and humans in each model compartment:
630 $S_m = 0.22$, $E_m = 0.29$, $I_m = 0.49$, $S_h = 0.58$, $E_h = 0.22$, $I_h = 0.00$, and $R_h = 0.20$. We
631 determined that the model was invariant to initial proportion values after a short burn-in
632 period (90 days) based on a sensitivity analysis (Fig. S10); therefore, we randomly
633 selected one set of initial proportion values from the sensitivity analysis for all the model
634 simulations. We also determined that the temporal trajectories of model dynamics did not
635 change when we varied the critical thermal minimum, maximum, and rate constants
636 (Table 4) for *Aedes aegypti* life history traits (Fig. S1-2).
637
638 We ran all model simulations using the deSolve package in R statistical software v 3.5.3
639 [79]. Model codes are available at https://github.com/jms5151/SEI-SEIR_Arboviruses.
640
641 Model validation
642 To validate the SEI-SEIR model, we calculated pairwise correlations with an adjusted p-
643 value to account for autocorrelation for each site. For the pairwise correlations, we used
644 the ccf function in base R [79] to calculate correlations between the two times series of

model predictions and observations with 0, 1, 2, 3, and 4-month lags. We then calculated an adjusted p-value using the Modified Chelton method [45] to adjust the null hypothesis test of sample correlation between autocorrelated time series. To assess predictions and observations for vector dynamics for each site, we compared monthly time series of the total predicted mosquito population from the SEI-SEIR model with the monthly time series of mean number of *Aedes aegypti* (per house). We followed the same procedure to compare model predictions with other mosquito life stages for sites in Kenya. Similarly, to compare predictions and observations for human disease dynamics for each site, we compared monthly times series of predicted infected individuals from the SEI-SEIR model with the monthly time series of total laboratory-confirmed arboviral cases. For subsequent analyses, we used model predictions from the model (e.g., SEI-SEIR model with a specific rainfall function and time lag) with the highest pairwise correlation value.

To compare key epidemic characteristics between model predictions and observations and to compare site-specific correlations with socio-economic factors, we used linear regression models using the lm function in that stats package in R [79]. We defined outbreaks as a continuous time period where the peak cases exceeded the median number of cases (predicted or observed) plus one standard deviation within a site. We then used those outbreak periods to count the total number of outbreaks within each site, and, for predicted and observed outbreaks that overlapped in time (or were slightly offset), the duration, peak timing, maximum number of infections, and total outbreak size. We compared predictions and observations for each of these metrics with linear regression. Since we were interested in whether model predictions matched observations for each

668 independent outbreak period, we did not allow varying intercepts or slopes by site.
669 Similarly, we compared the pairwise correlation values (described above) across all sites
670 with each socio-economic factor listed in Table 1 separately using linear regressions.
671
672 Comparison of R_0 with prior studies
673 We collected effect sizes of temperature on dengue incidence from 12 peer-reviewed
674 studies from the literature (Table S1). We selected studies with mean temperatures across
675 the predicted temperature range where arboviral transmission can occur. We scaled the
676 coefficient values to visualize the relative effect of temperature across studies given that
677 the original analyses were conducted with different temperature metrics and across
678 different temperature ranges. We provide additional information and sources in Table S1.
679
680 **Acknowledgements:** JMC, ADL, EFL, and EAM were supported by a Stanford Woods
681 Institute for the Environment – Environmental Ventures Program grant (PIs: EAM, ADL,
682 and EFL). EAM was also supported by a Hellman Faculty Fellowship and a Terman
683 Award. ADL, BAN, FMM, ENGS, MSS, ARK, RD, AA, and HNN were supported by a
684 National Institutes of Health R01 grant (AI102918; PI: ADL). EAM, AMSI, and SJR
685 were supported by a National Science Foundation (NSF) Ecology and Evolution of
686 Infectious Diseases (EEID) grant (DEB-1518681) and AMSI and SJR were also
687 supported by an NSF DEB RAPID grant (1641145). EAM was also supported by a
688 National Institute of General Medical Sciences Maximizing Investigators' Research
689 Award grant (R35GM133439) and an NSF and Fogarty International Center EEID grant

(DEB-2011147). We thank Cat Lippi for assistance with formatting household quality survey data from Ecuador.

Author contributions: EAM, ADL, EFL, and JMC conceived of project. JMC conducted analyses and wrote manuscript. EAM, ADL, EFL, and AMSI secured funding for the project. BNN, FMM, EBA, AA, MJBC, RD, FHH, RM, and HNN collected data. ENGS and MMS conducted laboratory analyses. ARK, SJR, and RS processed data. All authors revised and approved of the manuscript.

References:

1. Ockendon N, Baker DJ, Carr JA, White EC, Almond REA, Amano T, et al. Mechanisms underpinning climatic impacts on natural populations: altered species interactions are more important than direct effects. Glob Chang Biol. 2014;20: 2221–2229. doi:10.1111/gcb.12559
2. Boggs CL, Inouye DW. A single climate driver has direct and indirect effects on insect population dynamics. Ecol Lett. 2012;15: 502–508. doi:10.1111/j.1461-0248.2012.01766.x
3. Burkett VR, Wilcox DA, Stottlemyer R, Barrow W, Fagre D, Baron J, et al. Nonlinear dynamics in ecosystem response to climatic change: Case studies and policy implications. Ecol Complex. 2005;2: 357–394. doi:10.1016/j.ecocom.2005.04.010
4. Molnár PK, Sckrabulis JP, Altman KA, Raffel TR. Thermal Performance Curves and the Metabolic Theory of Ecology—A Practical Guide to Models and Experiments for Parasitologists. J Parasitol. 2017;103. doi:10.1645/16-148
5. Hortion J, Mutuku FM, Eyherabide AL, Vu DM, Boothroyd DB, Grossi-Soyster EN, et al. Acute Flavivirus and Alphavirus Infections among Children in Two Different Areas of Kenya, 2015. Am J Trop Med Hyg. 2019;100: 170–173. doi:10.4269/ajtmh.18-0297
6. Stewart-Ibarra AM, Lowe R. Climate and Non-Climate Drivers of Dengue Epidemics in Southern Coastal Ecuador. Am J Trop Med Hyg. 2013;88: 971–981. doi:10.4269/ajtmh.12-0478
7. Jury MR. Climate influence on dengue epidemics in Puerto Rico. Int J Environ

Health Res. 2008;18: 323–334. doi:10.1080/09603120701849836

8. Campbell KM, Haldeman K, Lehnig C, Munayco C V., Halsey ES, Laguna-Torres VA, et al. Weather Regulates Location, Timing, and Intensity of Dengue Virus Transmission between Humans and Mosquitoes. Michael E, editor. PLoS Negl Trop Dis. 2015;9: e0003957. doi:10.1371/journal.pntd.0003957

9. Adde A, Roucou P, Mangeas M, Ardillon V, Desenclos J-C, Rousset D, et al. Predicting Dengue Fever Outbreaks in French Guiana Using Climate Indicators. Scarpino S V., editor. PLoS Negl Trop Dis. 2016;10: e0004681. doi:10.1371/journal.pntd.0004681

10. Dhimal M, Gautam I, Joshi HD, O'Hara RB, Ahrens B, Kuch U, et al. Risk Factors for the Presence of Chikungunya and Dengue Vectors (Aedes aegypti and Aedes albopictus), Their Altitudinal Distribution and Climatic Determinants of Their Abundance in Central Nepal. Turell MJ, editor. PLoS Negl Trop Dis. 2015;9: e0003545. doi:10.1371/journal.pntd.0003545

11. Descloux E, Mangeas M, Menkes CE, Lengaigne M, Leroy A, Tehei T, et al. Climate-Based Models for Understanding and Forecasting Dengue Epidemics. Anyamba A, editor. PLoS Negl Trop Dis. 2012;6: e1470. doi:10.1371/journal.pntd.0001470

12. Aswi A, Cramb SM, Moraga P, Mengersen K. Epidemiology and Infection Bayesian spatial and spatio-temporal approaches to modelling dengue fever: a systematic review. Epidemiol Infect. 2018;147. doi:10.1017/S0950268818002807

13. Johansson MA, Apfeldorf KM, Dobson S, Devita J, Buczak AL, Baugher B, et al. An open challenge to advance probabilistic forecasting for dengue epidemics. Proc

759 Natl Acad Sci. 2019; 201909865. doi:10.1073/pnas.1909865116
760 14. Michael E, Singh BK, Mayala BK, Smith ME, Hampton S, Nabrzyski J.
761 Continental-scale, data-driven predictive assessment of eliminating the vector-
762 borne disease, lymphatic filariasis, in sub-Saharan Africa by 2020. BMC Med.
763 2017;15: 176. doi:10.1186/s12916-017-0933-2
764 15. Smith T, Maire N, Ross A, Penny M, Chitnis N, Schapira A, et al. Towards a
765 comprehensive simulation model of malaria epidemiology and control.
766 Parasitology. 2008. pp. 1507–1516. doi:10.1017/S0031182008000371
767 16. Ryan SJ, Carlson CJ, Mordecai EA, Johnson LR. Global expansion and
768 redistribution of Aedes-borne virus transmission risk with climate change. Han
769 BA, editor. PLoS Negl Trop Dis. 2019;13: e0007213.
770 doi:10.1371/journal.pntd.0007213
771 17. Kraemer MU, Sinka ME, Duda KA, Mylne AQ, Shearer FM, Barker CM, et al.
772 The global distribution of the arbovirus vectors *Aedes aegypti* and *Ae. albopictus*.
773 Elife. 2015;4. doi:10.7554/eLife.08347
774 18. Powell JR, Tabachnick WJ, Powell JR, Tabachnick WJ. History of domestication
775 and spread of Aedes aegypti - A Review. Mem Inst Oswaldo Cruz. 2013;108: 11–
776 17. doi:10.1590/0074-0276130395
777 19. Mordecai EA, Cohen JM, Evans M V., Gudapati P, Johnson LR, Lippi CA, et al.
778 Detecting the impact of temperature on transmission of Zika, dengue, and
779 chikungunya using mechanistic models. Althouse B, editor. PLoS Negl Trop Dis.
780 2017;11: e0005568. doi:10.1371/journal.pntd.0005568
781 20. Shocket MS, Ryan SJ, Mordecai EA. Temperature explains broad patterns of Ross

River virus transmission. Elife. 2018; doi:10.7554/eLife.37762.001

21. Paull SH, Horton DE, Ashfaq M, Rastogi D, Kramer LD, Diffenbaugh NS, et al. Drought and immunity determine the intensity of West Nile virus epidemics and climate change impacts. Proc R Soc B Biol Sci. 2017;284: 20162078. doi:10.1098/rspb.2016.2078

22. Costa EAP de A, Santos EM de M, Correia JC, Albuquerque CMR de. Impact of small variations in temperature and humidity on the reproductive activity and survival of Aedes aegypti (Diptera, Culicidae). Rev Bras Entomol. 2010;54: 488–493. doi:10.1590/S0085-56262010000300021

23. Gaaboub IA, El-Sawaf SK, El-Latif MA. Effect of Different Relative Humidities and Temperatures on Egg-Production and Longevity of Adults of Anopheles (Myzomyia) pharoensis Theob.1. Zeitschrift für Angew Entomol. 2009;67: 88–94. doi:10.1111/j.1439-0418.1971.tb02098.x

24. Koenraadt CJM, Harrington LC. Flushing Effect of Rain on Container-Inhabiting Mosquitoes Aedes aegypti and Culex pipiens (Diptera: Culicidae). J Med Entomol. 2009;45: 28–35. doi:10.1603/0022-2585(2008)45[28:FEOROC]2.0.CO;2

25. Paaijmans KP, Wandago MO, Githeko AK, Takken W, Vulule J. Unexpected High Losses of Anopheles gambiae Larvae Due to Rainfall. Carter D, editor. PLoS One. 2007;2: e1146. doi:10.1371/journal.pone.0001146

26. Benedum CM, Seidahmed OME, Eltahir EAB, Markuzon N. Statistical modeling of the effect of rainfall flushing on dengue transmission in Singapore. Reiner RC, editor. PLoS Negl Trop Dis. 2018;12: e0006935. doi:10.1371/journal.pntd.0006935

27. Stewart Ibarra AM, Ryan SJ, Beltrán E, Mejía R, Silva M, Muñoz Á. Dengue Vector Dynamics (Aedes aegypti) Influenced by Climate and Social Factors in Ecuador: Implications for Targeted Control. Mores CN, editor. PLoS One. 2013;8: e78263. doi:10.1371/journal.pone.0078263

28. Pontes RJ, Spielman A, Oliveira-Lima JW, Hodgson JC, Freeman J. Vector densities that potentiate dengue outbreaks in a Brazilian city. Am J Trop Med Hyg. 2000;62: 378–383. doi:10.4269/ajtmh.2000.62.378

29. Anyamba A, Linthicum KJ, Small JL, Collins KM, Tucker CJ, Pak EW, et al. Climate Teleconnections and Recent Patterns of Human and Animal Disease Outbreaks. Zhou X-N, editor. PLoS Negl Trop Dis. 2012;6: e1465. doi:10.1371/journal.pntd.0001465

30. Huber JH, Childs ML, Caldwell JM, Mordecai EA. Seasonal temperature variation influences climate suitability for dengue, chikungunya, and Zika transmission. Althouse B, editor. PLoS Negl Trop Dis. 2018;12: e0006451. doi:10.1371/journal.pntd.0006451

31. Lourenço J, Recker M. The 2012 Madeira Dengue Outbreak: Epidemiological Determinants and Future Epidemic Potential. Scarpino S V., editor. PLoS Negl Trop Dis. 2014;8: e3083. doi:10.1371/journal.pntd.0003083

32. Li R, Xu L, Bjørnstad ON, Liu K, Song T, Chen A, et al. Climate-driven variation in mosquito density predicts the spatiotemporal dynamics of dengue. Proc Natl Acad Sci. 2019;119: 3624–3629. doi:10.1073/PNAS.1806094116

33. Wang X, Tang S, Cheke RA. A stage structured mosquito model incorporating effects of precipitation and daily temperature fluctuations. J Theor Biol. 2016;411:

27–36. doi:10.1016/j.jtbi.2016.09.015

34. Siraj AS, Oidtman RJ, Huber JH, Kraemer MUG, Brady OJ, Johansson MA, et al. Temperature modulates dengue virus epidemic growth rates through its effects on reproduction numbers and generation intervals. Althouse B, editor. PLoS Negl Trop Dis. 2017;11: e0005797. doi:10.1371/journal.pntd.0005797

35. Oidtman RJ, Lai S, Huang Z, Yang J, Siraj AS, Reiner RC, et al. Inter-annual variation in seasonal dengue epidemics driven by multiple interacting factors in Guangzhou, China. Nat Commun. 2019;10. doi:10.1038/s41467-019-09035-x

36. Stewart-Ibarra AM, Muñoz ÁG, Ryan SJ, Ayala EB, Borbor-Cordova MJ, Finkelstein JL, et al. Spatiotemporal clustering, climate periodicity, and social-ecological risk factors for dengue during an outbreak in Machala, Ecuador, in 2010. BMC Infect Dis. 2014;14: 610. doi:10.1186/s12879-014-0610-4

37. Agha SB, Tchouassi DP, Turell MJ, Bastos ADS, Sang R. Entomological assessment of dengue virus transmission risk in three urban areas of Kenya. Reiner RC, editor. PLoS Negl Trop Dis. 2019;13: e0007686. doi:10.1371/journal.pntd.0007686

38. Agha SB, Tchouassi DP, Bastos ADS, Sang R. Dengue and yellow fever virus vectors: seasonal abundance, diversity and resting preferences in three Kenyan cities. Parasit Vectors. 2017;10: 628. doi:10.1186/s13071-017-2598-2

39. Chretien J-P, Anyamba A, Bedno SA, Breiman RF, Sang R, Sergon K, et al. Drought-Associated Chikungunya Emergence Along Coastal East Africa. Am J Trop Med Hyg. 2007;76: 405–407. doi:10.4269/ajtmh.2007.76.405

40. Vu DM, Mutai N, Heath CJ, Vulule JM, Mutuku FM, Ndenga BA, et al.

Unrecognized Dengue Virus Infections in Children, Western Kenya, 2014-2015. Emerg Infect Dis. 2017;23: 1915–1917. doi:10.3201/eid2311.170807

41. Gubler DJ, Nalim S, Saroso JS, Saipan H, Tan R. Variation in Susceptibility to Oral Infection with Dengue Viruses among Geographic Strains of Aedes Aegypti *. Am J Trop Med Hyg. 1979;28: 1045–1052. doi:10.4269/ajtmh.1979.28.1045

42. Xavier-Carvalho C, Chester Cardoso C, de Souza Kehdya F, Guilherme Pacheco A, Ozório Moraesa M. Host genetics and dengue fever. Infect Genet Evol. 2017;56: 99–110. doi:10.1016/J.MEEGID.2017.11.009

43. Didan K, Barreto Munoz A, Solano R, Huete A. MODIS Vegetation Index User's Guide (MOD13 Series) [Internet]. Available: http://vip.arizona.edu

44. Sulla-Menashe D, Friedl MA. User Guide to Collection 6 MODIS Land Cover (MCD12Q1 and MCD12C1) Product. 2018; doi:10.5067/MODIS/MCD12Q1

45. Pyper BJ, Peterman RM. Comparison of methods to account for autocorrelation in correlation analyses of fish data. Can J Fish Aquat Sci. 1998;55: 2127–2140. doi:10.1139/f98-104

46. Shocket MS, Anderson CB, Caldwell JM, Childs ML, Han S, Harris M, et al. Environmental drivers of vector-borne disease. Population Biology of Vector-borne Diseases. Oxford University Press;

47. Hurtado-Daz M, Riojas-Rodrguez H, Rothenberg S, Gomez-Dantes H, Cifuentes E. Impact of climate variability on the incidence of dengue in Mexico. Trop Med Int Heal. 2007;12. doi:10.1111/j.1365-3156.2007.01930.x

48. Colón-González FJ, Bentham G, Lake IR. Climate Variability and Dengue Fever in Warm and Humid Mexico. Am J Trop Med Hyg. 2011;84: 757–763.

doi:10.4269/ajtmh.2011.10-0609

49. Wang C, Jiang B, Fan J, Wang F, Liu Q. A Study of the Dengue Epidemic and Meteorological Factors in Guangzhou, China, by Using a Zero-Inflated Poisson Regression Model. Asia Pacific J Public Heal. 2014;26: 48–57. doi:10.1177/1010539513490195

50. Minh An DT, Rocklöv J. Epidemiology of dengue fever in Hanoi from 2002 to 2010 and its meteorological determinants. Glob Health Action. 2014;7: 23074. doi:10.3402/gha.v7.23074

51. Laureano-Rosario AE, Garcia-Rejon JE, Gomez-Carro S, Farfan-Ale JA, Muller-Kargera FE. Modelling dengue fever risk in the State of Yucatan, Mexico using regional-scale satellite-derived sea surface temperature. Acta Trop. 2017;172: 50–57. doi:10.1016/j.actatropica.2017.04.017

52. Wu P-C, Guoa H-R, Lung S-C, Lin C-Y, Su H-J. Weather as an effective predictor for occurrence of dengue fever in Taiwan. Acta Trop. 2007;103: 50–57. doi:10.1016/j.actatropica.2007.05.014

53. Karim MN, Munshi SU, Anwar N, Alam MS. Climatic factors influencing dengue cases in Dhaka city: a model for dengue prediction. Indian J Med Res. 2012;136: 32–9. Available: http://www.ncbi.nlm.nih.gov/pubmed/22885261

54. Nakhapakorn K, Tripathi N. An information value based analysis of physical and climatic factors affecting dengue fever and dengue haemorrhagic fever incidence. Int J Health Geogr. 2005;4: 13. doi:10.1186/1476-072X-4-13

55. Gharbi M, Quenel P, Gustave J, Cassadou S, Ruche G La, Girdary L, et al. Time series analysis of dengue incidence in Guadeloupe, French West Indies:

Forecasting models using climate variables as predictors. BMC Infect Dis. 2011;11: 166. doi:10.1186/1471-2334-11-166

56. Sharmin S, Glass K, Viennet E, Harley D. Interaction of Mean Temperature and Daily Fluctuation Influences Dengue Incidence in Dhaka, Bangladesh. Kasper M, editor. PLoS Negl Trop Dis. 2015;9: e0003901. doi:10.1371/journal.pntd.0003901

57. Sriprom M, Chalvet-Monfray K, Chaimane T, Vongsawat K, Bicout DJ. Monthly district level risk of dengue occurrences in Sakon Nakhon Province, Thailand. Sci Total Environ. 2010;408: 5521–5528. doi:10.1016/J.SCITOTENV.2010.08.024

58. Martínez-Bello D, López-Quílez A, Prieto AT. Spatiotemporal modeling of relative risk of dengue disease in Colombia. Stoch Environ Res Risk Assess. 2018;32: 1587–1601. doi:10.1007/s00477-017-1461-5

59. Mordecai EA, Caldwell JM, Grossman MK, Lippi CA, Johnson LR, Neira M, et al. Thermal biology of mosquito-borne disease. Byers J (Jeb), editor. Ecol Lett. 2019; ele.13335. doi:10.1111/ele.13335

60. Carrington LB, Armijos MV, Lambrechts L, Barker CM, Scott TW. Effects of Fluctuating Daily Temperatures at Critical Thermal Extremes on Aedes aegypti Life-History Traits. PLoS One. 2013;8. doi:10.1371/journal.pone.0058824

61. Ngugi HN, Mutuku FM, Ndenga BA, Musunzaji PS, Mbakaya JO, Aswani P, et al. Characterization and productivity profiles of Aedes aegypti (L.) breeding habitats across rural and urban landscapes in western and coastal Kenya. Parasit Vectors. 2017;10: 331. doi:10.1186/s13071-017-2271-9

62. Lowe R, Gasparrini A, Van Meerbeeck CJ, Lippi CA, Mahon R, Trotman AR, et al. Nonlinear and delayed impacts of climate on dengue risk in Barbados: A

modelling study. PLoS Med. 2018;15. doi:10.1371/journal.pmed.1002613

63. Li C, Wang X, Wu X, Liu J, Ji D, Du J. Modeling and projection of dengue fever cases in Guangzhou based on variation of weather factors. Sci Total Environ. 2017;605–606: 867–873. doi:10.1016/j.scitotenv.2017.06.181

64. Li CF, Lim TW, Han LL, Fang R. Rainfall, abundance of Aedes aegypti and dengue infection in Selangor, Malaysia. Southeast Asian J Trop Med Public Health. 1985;16: 560–8. Available: http://www.ncbi.nlm.nih.gov/pubmed/3835698

65. Johansson MA, Dominici F, Glass GE. Local and Global Effects of Climate on Dengue Transmission in Puerto Rico. Massad E, editor. PLoS Negl Trop Dis. 2009;3: e382. doi:10.1371/journal.pntd.0000382

66. Kenneson A, Beltrán-Ayala E, Borbor-Cordova MJ, Polhemus ME, Ryan SJ, Endy TP, et al. Social-ecological factors and preventive actions decrease the risk of dengue infection at the household-level: Results from a prospective dengue surveillance study in Machala, Ecuador. Messer WB, editor. PLoS Negl Trop Dis. 2017;11: e0006150. doi:10.1371/journal.pntd.0006150

67. Reich NG, Shrestha S, King AA, Rohani P, Lessler J, Kalayanarooj S, et al. Interactions between serotypes of dengue highlight epidemiological impact of cross-immunity. J R Soc Interface. 2013;10: 20130414. doi:10.1098/rsif.2013.0414

68. Wen J, Elong Ngono A, Regla-Nava JA, Kim K, Gorman MJ, Diamond MS, et al. Dengue virus-reactive CD8+ T cells mediate cross-protection against subsequent Zika virus challenge. Nat Commun. 2017;8: 1459. doi:10.1038/s41467-017-01669-z

69. Rodriguez-Barraquer I, Salje H, Cummings DA. Opportunities for improved surveillance and control of dengue from age-specific case data. Elife. 2019;8. doi:10.7554/eLife.45474

70. Stoddard ST, Forshey BM, Morrison AC, Paz-Soldan VA, Vazquez-Prokopec GM, Astete H, et al. House-to-house human movement drives dengue virus transmission. Proc Natl Acad Sci U S A. 2013;110: 994–999. doi:10.1073/pnas.1213349110

71. Wesolowski A, Qureshi T, Boni MF, Sundsøy PR, Johansson MA, Rasheed SB, et al. Impact of human mobility on the emergence of dengue epidemics in Pakistan. Proc Natl Acad Sci. 2015;112: 11887–11892. doi:10.1073/pnas.1504964112

72. Vaidya A, Bravo-Salgado AD, Mikler AR. Modeling climate-dependent population dynamics of mosquitoes to guide public health policies. Proc 5th ACM Conf Bioinformatics, Comput Biol Heal Informatics - BCB '14. 2014; 380–389. doi:10.1145/2649387.2649415

73. Schmidt CA, Comeau G, Monaghan AJ, Williamson DJ, Ernst KC. Effects of desiccation stress on adult female longevity in Aedes aegypti and Ae. albopictus (Diptera: Culicidae): results of a systematic review and pooled survival analysis. Parasit Vectors. 2018;11: 267. doi:10.1186/s13071-018-2808-6

74. Vazquez-Prokopec GM, Galvin WA, Kelly R, Kitron U. A New, Cost-Effective, Battery-Powered Aspirator for Adult Mosquito Collections. J Med Entomol. 2009;46: 1256–1259. doi:10.1603/033.046.0602

75. Waggoner JJ, Gresh L, Mohamed-Hadley A, Ballesteros G, Davila MJV, Tellez Y, et al. Single-Reaction Multiplex Reverse Transcription PCR for Detection of Zika,

Chikungunya, and Dengue Viruses. Emerg Infect Dis. 2016;22: 1295–7. doi:10.3201/eid2207.160326

76. Lanciotti RS, Calisher CH, Gubler DJ, Chang GJ, Vorndam A V. Rapid detection and typing of dengue viruses from clinical samples by using reverse transcriptase-polymerase chain reaction. J Clin Microbiol. 1992;30: 545–51. Available: http://www.ncbi.nlm.nih.gov/pubmed/1372617

77. Grossi-Soyster EN, Cook EAJ, de Glanville WA, Thomas LF, Krystosik AR, Lee J, et al. Serological and spatial analysis of alphavirus and flavivirus prevalence and risk factors in a rural community in western Kenya. Bingham A, editor. PLoS Negl Trop Dis. 2017;11: e0005998. doi:10.1371/journal.pntd.0005998

78. Palamara GM, Childs DZ, Clements CF, Petchey OL, Plebani M, Smith MJ. Inferring the temperature dependence of population parameters: The effects of experimental design and inference algorithm. Ecol Evol. 2014;4: 4736–4750. doi:10.1002/ece3.1309

79. Team RC. R: A Language and Environment for Statistical Computing. R Found Stat Comput. 2018; Available: https://www.r-project.org